Nanoscale

ROYAL SOCIETY OF CHEMISTRY

PAPER

View Article Online
View Journal | View Issue

Cite this: *Nanoscale*, 2025, **17**, 12894

Oleic acid rearrangement enables facile transfer of red-emitting quantum dots from hexane into water with enhanced fluorescence†

Tohid Baradaran Kayyal,[a] Jasper Tucker,[a] Chanda M. Lowrance,[a] Lekan Ajiboye,[a] Matthew Pelton,[a,b] Joseph W. Bennett[a] and Marie-Christine Daniel *[a]

Received 17th January 2025,
Accepted 23rd April 2025

DOI: 10.1039/d5nr00246j

rsc.li/nanoscale

There is significant demand for the conversion of hydrophobic nanoparticles (NPs) into water-soluble NPs, particularly for the transfer of photoluminescent quantum dots (QDs) synthesized in organic solvents into water-based settings. However, these transfer processes are often inefficient, with only a fraction of the QDs transferred into water, and typically result in decreases in photoluminescence quantum yield (PLQY). Here, we demonstrate a straightforward technique to efficiently transfer oleic acid (OA)-coated CdSe/CdS core–shell QDs into water without the addition of any new reagents. In contrast to the decrease in PLQY that is usually observed when QDs are transferred into water, this process in fact leads to an increase of the PLQY after transfer in basic water (pH 8). The process is highly reproducible and can be applied to other oleic acid-coated NPs. Density-functional-theory (DFT) calculations indicate that the QD transfer into water is enabled by the rearrangement of OA ligands at the surface of the QDs. This discovery allows for widely available, hydrophobic OA-coated QDs to be used in water media without any further modification and with enhanced fluorescence.

Introduction

Nanoscale semiconductor crystals, or quantum dots (QDs), possess unique optical and electronic characteristics resulting from size-dependent quantum confinement, which makes them superior candidates for a wide range of applications.[1–3] As fluorophores, QDs offer numerous advantages over organic dyes, including high photostability, broad excitation spectra, narrow and bright emission, long fluorescence lifetime, and size-tunable optical properties,[3–6] which allow for multiplex imaging and tracking of biological species with enhanced accuracy and sensitivity.[5,7] In addition, QDs are playing a significant role in photonics, optoelectronics, and quantum computing.[8–11] Among many types of QDs, CdSe-based QDs are the most frequently utilized owing to their extensive development history and capacity to provide bright, size-tunable emission across the visible spectral range.[12,13]

CdSe QDs are most commonly synthesized using an organic solvent-mediated approach in which highly controlled reaction conditions (*e.g.*, the hot injection method) lead to uniform size distribution, well-defined shape, and high crystallinity of the synthesized QDs.[12] While this conventional preparation of CdSe QDs in organic solvents leads to lipophilic QDs, there is a need for water-soluble QDs, not only for biomedical imaging, but also in the domain of photonics, where CdSe QDs are combined with metal nanoparticles (NPs) such as gold NPs (natively prepared in aqueous media) for the development of novel hybrid materials.[14] Therefore, it is crucial to be able to efficiently transfer CdSe QDs that were synthesized in an organic solvent into water media in a way that can preserve their high quality, especially their high photoluminescence quantum yield (PLQY).

Two main approaches have emerged as dominant strategies for transferring QDs from organic solvents to aqueous media, namely ligand exchange and encapsulation.[14–16] Ligand exchange relies on replacing the original hydrophobic ligands on the surface of QDs with hydrophilic ligands, resulting in the QDs becoming water-soluble.[14,17–19] A significant drawback

[a]*Department of Chemistry and Biochemistry, University of Maryland Baltimore County (UMBC), Baltimore, Maryland 21250, USA. E-mail: mdaniel@umbc.edu*
[b]*Department of Physics, University of Maryland Baltimore County (UMBC), Baltimore, Maryland 21250, USA*

† Electronic supplementary information (ESI) available: Absorption and emission spectra, as well as FTIR spectra and lifetime measurements of QDs in Millipore water, photostability of the transferred QDs, properties of the transferred QDs in acidic environment, ionic strength effect on QDs transfer, absorption and emission spectra of QDs in borate buffer, data from control studies, depiction of carboxylic acid ligands, depiction of CdS surfaces, additional adsorption energy measurements, additional depictions of ligand orientations on CdS surfaces, distances of vertical *cis*-isomer ligands in dimer and opposite hexamer systems, injected volumes of the Cd and S precursors during the formation of the CdS shell. See DOI: https://doi.org/10.1039/d5nr00246j

of the ligand exchange process is that the exchange reaction is often incomplete or inefficient, leading to poor exchange yield and/or QD aggregation.[14] By contrast, encapsulation methods use a protective shell or coating material that surrounds the QD core and provides stability in an aqueous environment.[14] Encapsulation materials include silica shells,[16,20,21] polymer coatings,[16,22,23] and micelles[14,24,25] and solid–lipid structures.[26] However, these techniques also suffer from some limitations in that the PLQY and stability of QDs can be significantly decreased due to limited control over the thickness, uniformity, and composition of the shell around the QDs. In addition, the overall dimensions of QDs can be significantly increased by encapsulation methods, which can impose constraints on their potential applications.[16,27] Moreover, multiple steps are required to purify and isolate the QDs from excess coating materials or byproducts. Despite these deficiencies, ligand exchange and encapsulation strategies remain the most effective ways to date for transferring QDs from organic solvents to aqueous media.

Here, we report the transfer of CdSe/CdS core–shell QDs coated with oleic acid (OA) from hexane into aqueous media through a facile, one-step method using ultrasonic assistance, without addition of any further reagent or surface modification. Surprisingly, instead of the decrease of PLQY typically found when QDs are transferred from organic to aqueous phase, an enhancement of PLQY was observed after transfer into basic water. We also found that the same process can be used for other OA-coated NPs, such as OA-coated magnetite NPs. This finding will allow for conventional hydrophobic OA-capped NPs to be readily handled in aqueous media while maintaining superior optical quality.

The novelty of this work resides in the fact that this reported water-transfer process is a new process that does not rely on encapsulation nor on ligand exchange reaction, since we do not introduce any new ligands (including any additional OA ligands) during transfer into water. We hypothesize that water solubility is enabled by a rearrangement of some of the original OA ligands at the surface of QDs that results in a mixed monolayer in which some of the OA ligands remain with their carboxylic acid heads attached to the QD surface while the remaining OA ligands have their carboxylic acid groups facing the surrounding water. We investigated this hypothesis using first-principles density functional theory (DFT) modeling. These models showed that the ligand rearrangement is an energetically favorable configuration and results in the creation of a new hydrogen bonding network. Moreover, DFT was used to extend the experimental work by investigating adsorption of (i) *trans*-alkene isomers and (ii) a mix of *cis* and *trans*-alkene isomers to understand the influence of isomerism and isomer packing on carboxylic acid surface adsorption energies. To the best of our knowledge, this work is the first study involving the transfer of nanoparticles into water through the rearrangement of ligands already present on the nanoparticles.

This paper is comprised of two main sections: experimental studies and DFT calculations for the presented aqueous transfer of OA-coated NPs.

Results and discussion

Single-phase strategy for hydrophobic NP transfer into aqueous solution

We developed a straightforward, single-phase method for the efficient transfer of OA-coated NPs from organic to aqueous media. The NPs are removed from the organic solvent, forming either a pellet (in the case of QDs) or a dried powder (in the case of Fe_3O_4 magnetic NPs). Water (either Millipore water or basic water) is directly added to the pellet or powder, followed by sonication. The NPs progressively form a stable suspension in the aqueous media (4 hours for QDs and 3 days for magnetite NPs).

Efficient transfer of QDs into aqueous solution

The majority of our study focuses on OA-coated CdSe/CdS QDs. In this case, the QDs were centrifuged in order to concentrate them into a pellet and to remove the organic solvent. The addition of water to the QD pellet first resulted in a cloudy solution. This initial cloudiness is attributed to a temporary aggregation, which is caused by the original lack of water solubility of the QDs. By sonicating for 2 minutes every hour over a total of 4 hours, the QDs solution in aqueous media became clearer over time with ultimately no cloudiness remaining. In contrast with previously reported water-transfer methods, in our study no additional ligands or surfactants were added to the aqueous solution. Therefore, the transfer of QDs into water can only be due to a rearrangement of OA at the surface of the QDs. We hypothesize that some of the OA ligands invert at the surface of the QD, now exposing the carboxylic heads to the aqueous environment, rendering the QDs hydrophilic. It is important to note that, while the inverted OA ligands may not be coordinated to metal atoms through their carboxylic acid ends anymore after transfer into water, the resulting water solubility of the QDs implies that the flipped OA remain at the QD surface. In addition, our DFT studies show that the methyl ends of the flipped OA ligands interact with the QD surface through outer sphere adsorption, and that the flipped OA ligands are further stabilized at the QD surface through interaction with neighboring ligands (*vide infra*). Fig. 1 illustrates the hypothesized OA ligand rearrangement.

Although other mechanisms may be considered, the hypothesis of micelle formation being responsible for QD transfer into water has been excluded because OA does not form micelles at pH < 9,[28] which is the case of our study (5.5 < pH < 8). Similarly the formation of oil-in-water droplets is not being considered as the reason for QD transfer into water because the size of OA oil-in-water droplets is very large compared to our QDs (>1000 nm *versus* 13 nm):[28] if such droplets were forming in our study, we would observe large groups of QD per droplet,[26] but instead we mostly see dispersed single QDs (*vide infra*: Fig. 3a).

Fig. 2a shows the absorption spectra of CdSe/CdS QDs after redispersion into basic water (pH 8) as a function of time. As can be seen, the initially high absorbance background due to the scattering of aggregates gradually decreases during the

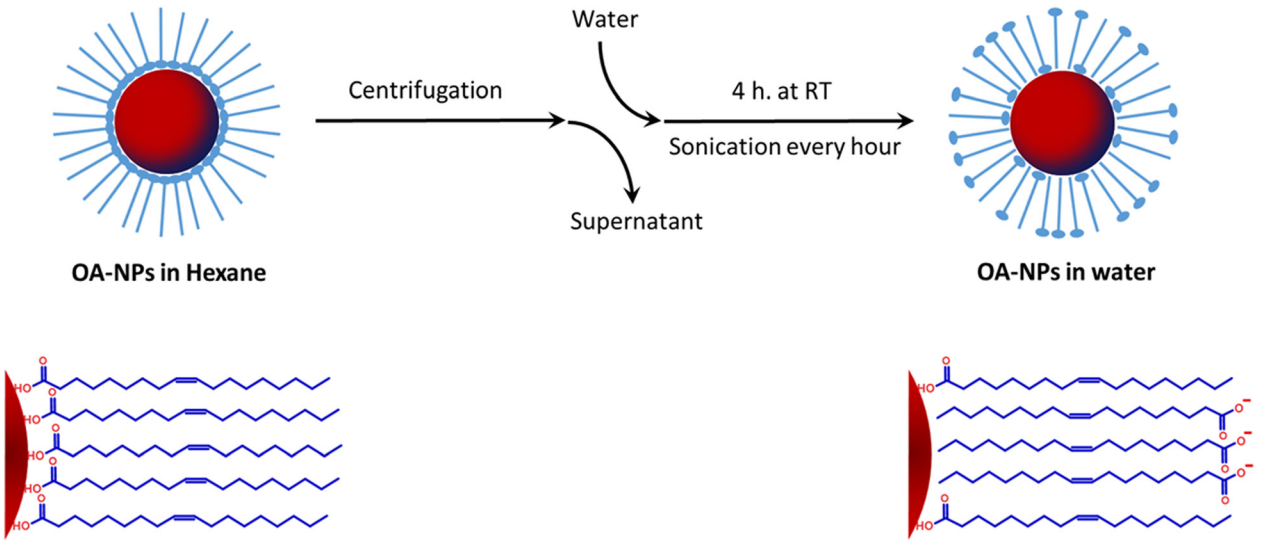

Fig. 1 Illustration of nanoparticle transfer from hexane to water through the rearrangement of oleic acid capping molecules.

solubilization of the QDs in water media, and it stabilizes close to zero after about 4 h. This means that the initial aggregation of QDs after addition of water decreases with time and the QDs become more and more soluble in water. A similar behavior is observed when using Millipore water as the transfer medium (Fig. S1a†). Furthermore, Fig. 2b demonstrates that the absorption spectrum of the QDs recovered in water media is very similar to the spectrum of the QDs redispersed in hexane, with the first exciton staying at the same wavelength. This indicates that the QD core is unchanged by the transfer process. In addition, the difference in absorbance at 450 nm shows that a high yield of QD recovery in basic water (about 80%) is obtained through this transfer method.

The same ability to disperse QDs in aqueous media was obtained for over fifty independent experiments, indicating a high degree of reproducibility for this transfer method. The reproducibility of the QD transfer process is ensured by preventing pellet from drying before adding basic water, by starting the first sonication cycle immediately after the water addition, and by adjusting the pH of water when it is added to the QDs pellet.

Photoluminescence enhancement of QDs after transfer into aqueous media

The photoluminescence (PL) spectra of CdSe/CdS QDs in hexane and basic water (pH 8) are presented in Fig. 2c, and photographs of the samples under UV illumination are displayed in Fig. 2d; all sample volumes were adjusted to have an absorbance of 0.1 at the excitation wavelength (470 nm). In contrast to most previous studies, which have typically reported a significant decrease in QD photoluminescence (PL) intensity following transfer from organic solvents to aqueous media, in this study a significant increase in PL intensity was observed upon QDs transfer into basic water while a stable PL intensity was observed upon QD transfer into Millipore water (Fig. S1b†).

In addition, fluorescence lifetime measurements were carried out (Fig. S2†) and only a very small change was observed between the PL decay of QDs before and after transfer into water.

In general, the fluorescence quenching typically occurring in water has been attributed to high-energy vibrations of functional groups (*i.e.*, hydroxyl moieties or other heteroatom-containing groups) and high polarity of the solvent, which can cause non-radiative and intramolecular energy transfer.[29,30] However, in our study, no net quenching of PL is observed, even when using Millipore water. Following our hypothesis of OA ligand rearrangement, one reason for the higher than usual PL in water media could be a decrease in the number of carboxylic acid heads coordinated to the surface of QDs. The carboxylic acid heads of the OA molecules can act as electron-withdrawing functional groups, lowering the number of photons emitted; reorienting the OA molecules can reduce the electron-withdrawing effects and ultimately leads to an increase in fluorescence efficiency.[31]

Fluorescence quenching can also occur upon transfer into water due to partial aggregation of the QDs. When QDs are transferred into basic water using our method, the proposed OA ligand rearrangement leads to the formation of a significant number of carboxylate anions at the surface of each QD; this interpretation is supported by the highly negative zeta potential value (−69 mV) of the QDs in basic water. This large surface charge stabilizes the QD colloid through electrostatic repulsion, minimizing particle aggregation. In Millipore water, the surface charge is lower, and a certain degree of aggregation may occur, resulting in somewhat lower fluorescence intensity as compared to QDs in basic water.

The electrostatic stabilization of QDs in basic water is also supported by their high degree of colloidal stability. Indeed,

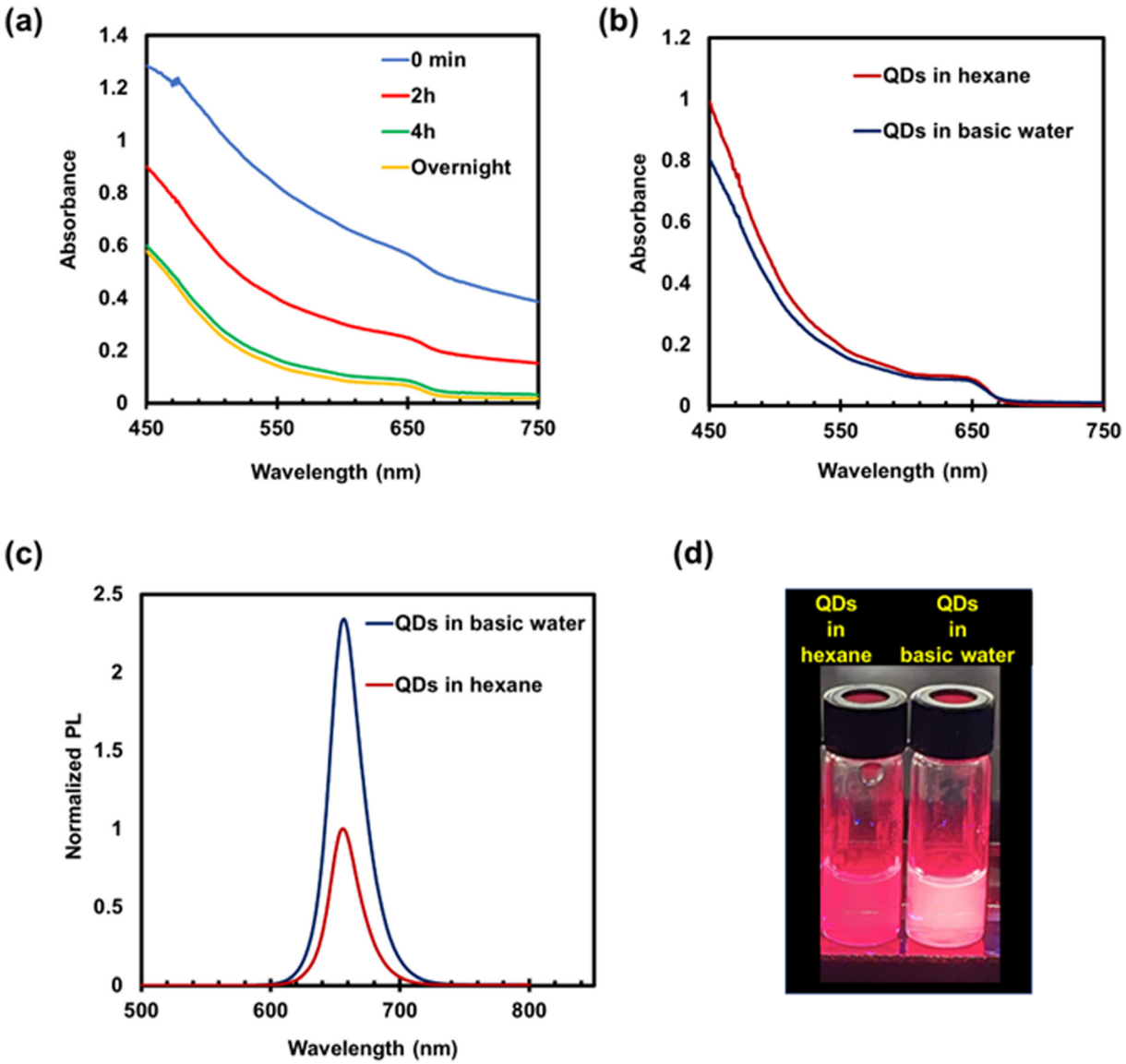

Fig. 2 (a) Absorption spectra of oleic-acid (OA)-capped quantum dots (QDs) after redispersion into aqueous media (pH 8) as a function of time. (b) The comparison of QD absorbance in hexane *versus* after complete redispersion into basic water (pH 8). (c) Emission spectra of OA-capped QDs in hexane and after transfer into basic water. (d) Photographs of QDs under UV light illumination (365 nm) in hexane (left) and in pH 8 water (right).

the PL intensity of the QDs was not measurably changed for two weeks after transfer into basic water and decreased by only 10% over two months (Fig. S3†).

A significant improvement in the photoluminescence quantum yield (PLQY) was observed in the red-emitting QDs upon transfer into pH 8 water (PLQY calculations were done using eqn (S1)†). A batch of QDs with a low initial PLQY (QDs 1) was first used: in this case, the PLQY improved from 17% in hexane to 38% upon transfer to basic aqueous media (Table 1). A second batch of red-emitting QDs with higher initial PLQY of 46% in hexane (QDs 2), displayed a PLQY of 63% upon transfer to pH 8 water (Table 1). The absorbance and emission spectra of QDs 2 in hexane and after transfer to basic water are shown in Fig. S4.†

Table 1 Photoluminescence quantum yields (PLQY) of two different batches of oleic-acid-capped CdSe/CdS quantum dots (with different initial PLQY) redispersed in hexane and basic water (pH 8). The PLQY were quantified using tetraphenylporphyrin (TPP) as a reference, with PLQY(TPP) = 7%

	PLQY (%)	
Solvent	Hexane	Basic water (pH 8)
QDs 1	17	38
QDs 2	46	63

It is important to note that the goal of this study is not to report the highest possible PLQY of CdSe/CdS QDs in water. Instead, it focuses on demonstrating that OA ligands can

rearrange around NPs to enable efficient transfer of QDs from organic to aqueous media, with PLQY higher than for the same QDs in their original organic solvent. Typically, even QDs with very high PLQY (>90%), such as those synthesized using Bawendi's well-known method,[6] experience a substantial drop (around 20%) in PLQY upon transfer to water using common ligand exchange strategies. Considering this drop, a final PLQY of 63%, as reported here, is thus comparable to the best reported values for red-emitting QDs in water. This result is achieved using a facile method, without the need for any further surface modifications.

Characterization of transferred QDs in basic water

Transmission electron microscopy (TEM) images, such as the one shown in Fig. 3a, demonstrate that the transferred QDs were effectively redispersed in water media while maintaining their individual, single QD structure and overall morphology. An average size of 13.4 ± 1.7 nm was determined by TEM analysis (400 particles counted). Additionally, the QDs were analyzed by Dynamic Light Scattering (DLS), which indicated an average hydrodynamic diameter of approximately 19 nm in solution, including the length of OA ligands (Fig. S5†). However, due to the QDs' red emission closely aligning with the 633 nm laser wavelength used in the DLS system, there is potential for interference that could affect the accuracy of the reported size distribution. The formation of an electric double layer at the nanoparticle surface in water can also contribute to the increase in the hydrodynamic diameter. Importantly, despite the high sensitivity of DLS to aggregation, no peak corresponding to aggregation or agglomeration of QDs was observed after transfer to water.

In addition, a diluted solution of the QDs transferred in water was deposited onto a substrate, and bright PL was readily observed from single QDs. For single-QD PL measurements, the QDs were deposited on a glass substrate at a concentration much lower than that used to prepare the TEM grids. Several single-QD spectra were measured, and a representative result is shown in Fig. 3b. Each individual QD exhibits a narrow, single peak, and the width of this peak corresponds to the homogeneous linewidth expected for a single QD at room temperature. The observed QDs also all exhibited blinking, characteristic of single, isolated nanocrystals.

Finally, FTIR analyses were carried out. The FTIR spectra of OA-capped CdSe/CdS QDs before and after aqueous transfer display significant changes (Fig. S6†). The main difference in the spectra is due to the formation of hydrogen bonding of the OA carboxyl groups in the aqueous medium, which appears as a broad peak around 3400 cm^{-1}. This results from ligand rearrangement, where deprotonated carboxyl groups face the solvent. The disappearance of the C═O band at 1720 cm^{-1} and the appearance of COO^- stretching bands at 1550–1640 cm^{-1} confirm the formation of carboxylate anions. Moreover, the general broadening of the peaks in the FTIR spectrum after transfer into water may reflect the presence of the two different orientations of OA on the QD surface. Thus, the FTIR data provide clear evidence of ligand rearrangement on the surface after aqueous transfer.

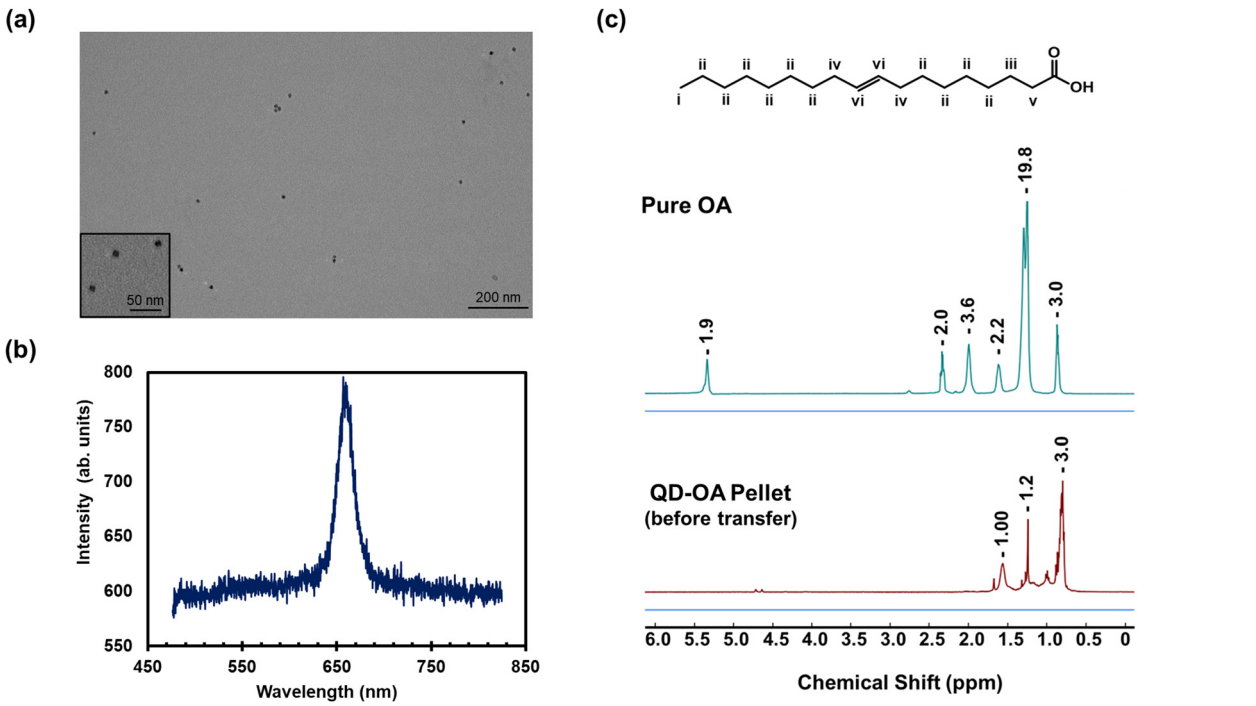

Fig. 3 (a) Representative TEM image of oleic-acid (OA)-capped quantum dots (QDs) transferred to basic water (inset: higher magnification image of QD-OA). (b) Sample photoluminescence spectrum of a single QD deposited on a substrate after being dispersed in basic water. (c) ^1H NMR spectra of pure OA and OA-capped QDs pellet (before transfer into basic water) in $CDCl_3$.

Control: biphasic strategy for the transfer of QDs into water

Biphasic strategies are commonly used to transfer QDs from organic to aqueous phases. In these methods, free ligands are added in order to form a bilayer around the surface of the QDs. In our study, there is no addition of free ligands or surfactants to the QD organic solution or to the water. In order to compare the biphasic approach to our strategy for QD transfer into water, we attempted to transfer the synthesized hydrophobic OA-coated QDs into water media using a biphasic strategy similar to the one developed by Prakash *et al.*,[24] but without adding any additional ligands. 1 mL of QDs in hexane was added to 10 mL water, followed by 5 min sonication to create an emulsion. A cloudy solution was obtained after sonication, and it sat undisturbed for one day. After the separation of the two phases, it was observed that the top layer (QDs in hexane) remained yellow in color while the aqueous phase was still colorless (Fig. S7†). The absorption spectra of the hexane layer were studied before and after mixing with water, and it was determined that only about 10 percent of the QDs were transferred into the water. The results clearly indicate that the presence of additional free ligands is critical to allow for the transfer of QDs in water using the biphasic method.

By contrast, no additional free ligands are added for our new transfer strategy. In our method, the QDs are extracted at least 5 times using methanol followed by centrifugation. Any free ligands remaining at this point would be too little to be responsible for the roughly 80% efficiency of aqueous transfer that we observed using our method. To further rule out the potential role of free ligands in the transfer to aqueous solution, we dissolved the QD pellet in chloroform (prior to transfer into water) and measured the NMR spectrum, compared to that of pure OA. As illustrated in Fig. 3c, the environment of OA protons was strongly affected by the QD cores. Indeed, when organic ligands are bound to the surface of a colloidal inorganic nanoparticle, the ^{1}H NMR peaks of the bound ligands significantly broaden, and can also be shifted downfield. This is due to the fact that those protons have a short T_2 relaxation time, faster than the delay required to extract the Brownian diffusion.[32] The broadening is typically more pronounced for protons closer to the nanocrystal surface.[33,34] The extent of the broadening also depends on the size of the nanoparticle: as the NP size increases, the broadening increases, to the point of peak loss.[35] Since the QDs in our study are relatively large (about 13 nm diameter), there is a strong effect on the ^{1}H NMR peaks of the surface-bound OA, which results in the majority of the OA protons no longer showing a measurable peak. Specifically, in Fig. 3c, the signals of the protons next to the carboxylic groups (peak v) and of the central double bond of the OA structure (peaks iv and vi) were absent in the NMR spectrum of QD-OA. In addition, there was a significant reduction in the intensity of methylene (CH_2) peaks for OA in the QD sample compared to pure OA ligand. The methyl (CH_3) peak remained in the NMR spectrum of the QDs; the methyl protons are much less affected by the QD core because they are the farthest away from the core in chloroform. These spectral changes verify both the attachment of OA onto the QD surfaces and the absence of any significant amount of free OA within the sample.

Effect of pH and ionic strength on QD dispersion in water

The QD transfer into aqueous media is pH-dependent and does not occur in an acidic environment. Fig. S1a† shows the absorbance of QDs after transfer to Millipore water (pH 6) as a function of time. A similar behavior was observed as with basic water (pH 8); however, a thorough comparison of Fig. S1a† with Fig. 2a reveals that the absorbance at 450 nm was lower, and the background at 750 nm was higher at pH 6. This indicates that the recovery of QDs was less efficient in Millipore water (pH 6) than in basic water (pH 8). Fig. S1b† also shows the emission of QDs in Millipore water (pH 6) compared to QDs in hexane, with both absorbance adjusted to 0.1 at the excitation wavelength (470 nm) for comparison purpose. The fluorescence intensity of QDs in Millipore water was similar to that in hexane, with no significant enhancement, which is in contrast to the improvement in fluorescence intensity observed for QDs in basic water. The transfer of QDs into an acetate buffer solution (pH 4) was also investigated; however, complete aggregation was observed in this medium (Fig. S8a†).

The observed pH-dependent behavior of QD transfer can be further understood by examining the surface charge of the QDs. Zeta potential measurements revealed a value of −69 mV at pH 8, whereas at pH 6, the value was −30 mV. The more highly negative zeta potential in the basic environment suggests greater electrostatic repulsion, which enhances the colloidal stability of the QDs. Additionally, this indicates that more rearrangement of OA ligands has occurred in basic water than at pH 6, contributing to the observed enhancement in the optical properties of the transferred QDs. On the other hand, the aggregation at pH 4 is due to a lack of adequate charges needed for electrostatic repulsion between NPs in water (zeta potential = 1.3 mV). This is also consistent with insufficient OA ligand inversion at lower pH. The observed pH dependency thus supports the hypothesis of a rearrangement of the OA molecules on the QD surface, with more basic environments favoring greater rearrangement. As a note, although it has been found that the surface of CdS shells is Cd-rich (59% Cd *versus* 41% S),[36] the cation : anion (Cd^{2+} : S^{2-}) ratio inside the QD shells is 1 : 1 (equimolar amounts of cadmium and sulfur precursors are used during the shell growth Xie *et al.*,[37] Li *et al.*[38] and Hanifi *et al.*[39]), so the shell is overall neutral and the overall zeta potential only corresponds to charges from OA ligands.

The effect of the ionic strength of the aqueous media used for QD transfer was also investigated. Increasing the ionic strength of the aqueous media over 50 mM inhibits QDs transfer from hexane into water: as depicted in Fig. S8b,† there is no transfer of QDs to water media after redispersing into high ionic strength solutions such as PBS buffer (1×, pH 8, 150 mM). However, lower ionic-strength solutions of alkaline media (pH 8, ≤50 mM, using KOH or $NaHCO_3$) do not inter-

fere with QDs dispersion into water. In addition, a borate buffer solution at pH 8 and concentration of 50 mM was identified as a suitable buffer medium for the transfer of QDs, given that it resulted in good recovery (about 65%) and strong fluorescence intensity (Fig. S9†). Although it is not possible to directly transfer the QDs into PBS buffer solutions, it is noteworthy that, after QDs are transferred into aqueous media, they demonstrate colloidal stability when mixed with PBS. Indeed, upon adding PBS, the QDs maintain stability for more than a week in 0.1× PBS and for more than 12 hours in 1× PBS, without any precipitation, significant changes in their UV-Vis absorbance spectra, or evidence of aggregation (Fig. S10†).

Effect of pellet dryness on redispersion

QD transfer from organic to aqueous media was carried out directly on QD pellets collected after centrifugation. However, it appeared to be important not to let the pellet dry completely before adding basic water. Fig. 4a illustrates the results of respectively adding water and hexane to dried QD pellets. The completely dried pellets are not able to transfer into a water medium, whereas they readily redisperse in hexane after a few seconds of sonication. One possible explanation could be that the QDs are highly packed when dried into a film, which leads to hydrophobic interactions among OA ligands of different QDs; this, in turn, prevents access of solvent to the surface of QDs for deprotonation of the carboxylic groups and subsequent OA rearrangement.

Repeated redispersion in aqueous media

In order to assess the stability of the newly water-soluble QDs, we investigated the possibility of redispersing these QDs into solvent a second time. The already redispersed QDs in basic water were centrifuged again, and either basic water or hexane was added to the pellets. Upon the addition of basic water to the pellet, the resulting solution displayed a similar absorption profile to that observed after the first redispersion, as shown in Fig. 4b. The slight decrease in absorbance can be related to some QD loss in the supernatant after the second centrifugation. On the other hand, the addition of hexane to the pellet did not result in any observable redispersion (Fig. 4c). It can be thus concluded that the recovered QDs after transfer into basic water cannot be transferred back into hexane, which indicates that the rearrangement of OA ligands is irreversible.

Transfer of magnetic Fe_3O_4 NPs into aqueous media

In order to assess the generality of the aqueous transfer method, we used the same approach to redisperse purified OA-coated magnetite (Fe_3O_4) NPs in aqueous media. Unlike QDs, magnetite NPs were obtained as a powder at the end of their synthesis; water was thus added directly to this powder. The magnetite NPs gradually resuspended into pH 8 water, but it took a longer time than for the QDs (3 days *versus* 4 hours, respectively), as shown in Fig. 5a. Despite the slow kinetics of the rearrangement, this finding reveals that the rearrangement of OA ligands can occur for other types of NPs without adding any free OA molecules. The extended time for transfer can be attributed to the higher hydrophilicity of the magnetite surface compared to the CdS surface; this means that the interaction between the surface and deprotonated carboxylic group is less unfavorable, and thus the OA ligands rearrange more slowly. We also note that the magnetite NPs could be redispersed in water when starting as a dried powder, in contrast to the case of dried QD pellets; this is most likely because the solvent can more readily access the NP surfaces in the powder compared to the tightly packed QD pellet that dries as a film.

Zeta potential measurements were also conducted for magnetite NPs transferred to basic water (pH 8) and Millipore

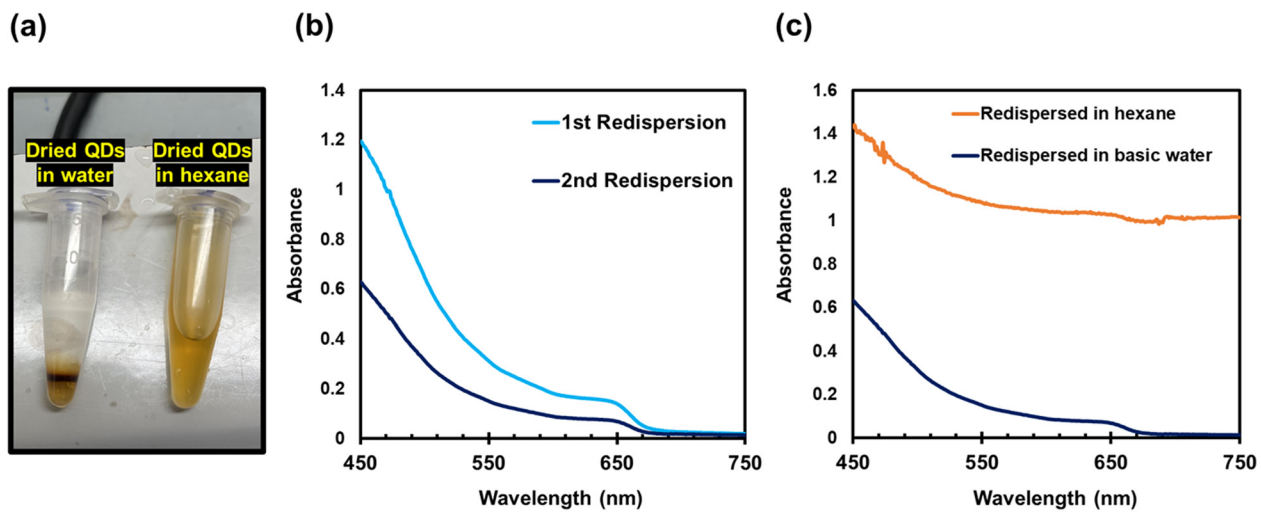

Fig. 4 (a) Photograph of dried pellets of oleid-acid-capped quantum dots (QDs) redispersed in water (left) and hexane (right). (b) Absorption spectra of the water-soluble QDs after a first and second redispersion in basic water. (c) Absorption spectra of the water-soluble QDs after a second redispersion in basic water and in hexane, after first being redispersed in basic water.

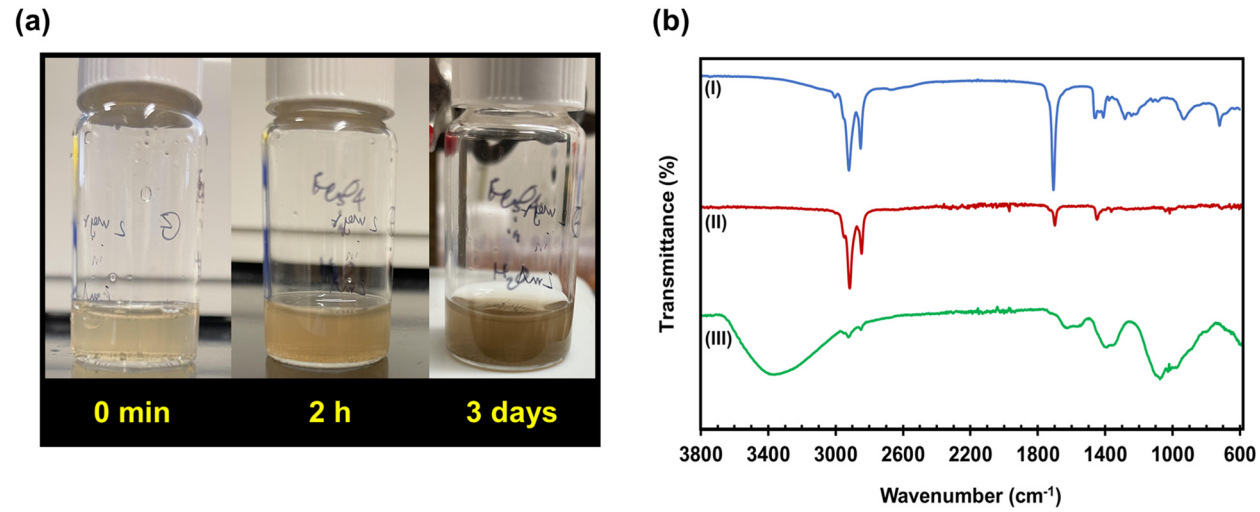

Fig. 5 (a) Photographs of oleic-acid (OA)-coated magnetite nanoparticles (NPs) transferred into pH 8 water as a function of time. (b) FT-IR spectra of pure OA ligands (I), OA-coated magnetite NPs in hexane (II), and OA-coated magnetite NPs after transfer into water (III).

water (pH 6), giving values of −48 mV and −37 mV, respectively. The difference in zeta potential value between basic water and Millipore water is smaller for magnetite NPs than for QDs, which can likely be ascribed to the higher affinity of carboxylate groups to the surface of magnetite NPs.

Fig. 5b compares the FT-IR spectra of magnetite NPs suspended in water to those of magnetite NPs suspended in hexane as well as to pure OA ligands. The main differences in spectra originate from the hydrogen bond formation of carboxyl groups in aqueous media, which appears as a broad characteristic peak in the range of 3200 to 3500 cm^{-1}. The hydrogen bond formation in water can occur for the OA ligands due to their rearrangement (carboxyl groups facing the NP surface deprotonate, flip, and then face the solvent). The presence of asymmetric peaks in the range of 1550 to 1640 cm^{-1} may be related to the formation of carboxylate anions in water media. The results obtained from FT-IR analysis thus provide further evidence for the ligand rearrangement that occurs at the surface of the NPs. In addition, the FT-IR profile of Fe_3O_4 NPs after transfer to water is very similar to the one observed for QD-OA (Fig. S6†), which is expected since FT-IR analysis focuses mostly on the organic part of the sample.

Computational studies supporting the proposed mechanism of QD transfer into water

Before modeling the complex surface rearrangement discussed in the previous sections, first-principles methods were used to determine basic surface-adsorbate parameters of small chain carboxylic acids interacting with CdS surfaces (CdS is the shell of the QD). These parameters include adsorption energy and adsorption geometry, which includes site preferences, and distances from the surface. Specifically, DFT studies were first initialized with a single adsorbate in multiple potential binding configurations then allowed to fully relax, in order to assess the fully relaxed atomistic geometries as well as the strength of surface interactions.

Since the proposed rearrangement includes both ends of an aliphatic carboxylic acid interacting with a surface, we include both configurations in our test set, and since pH variations in preparation also influence experimentally observed behaviors, we also included structures where the carboxylic acid is deprotonated to understand how protonation state, surface structure, and ligand packing density could influence each other and collective adsorption properties. This information was then used to rank the types of ligand–surface interactions that might be observed and then informed the next sets of calculations, which kept increasing in complexity.

The computational analysis presented here goes from a single adsorbate to two adsorbates, and finally six adsorbates, to produce the energetics of pairwise, and ultimately multiple pairwise atomistic interactions, which could provide a closer match to experimental results by modeling more realistic ligand packing densities. The data that is tabulated is the adsorption energy of specific configurations, as well as corresponding bond lengths, and ligand–surface distances.

Here we took a reductionist approach to modeling surface–adsorbate interactions to generate atomistic information in this initial investigation. All DFT calculations presented here are performed in vacuum, without the inclusion of implicit solvation or the addition of explicit water molecules (which are beyond the scope of the current study). The DFT simulations were performed without the addition of water molecules to better understand the extent of hydrogen bonding between the ligands themselves. These simulations varied the number of ligands, their orientations, and used *cis* and *trans* isomers, to map the breadth of this broadly applicable effect. Given that the hydrogen bonding between the ligands themselves is present in our calculations, in vacuum, the hydrogen bonding would only increase in the presence of additional water molecules.

(a) Single adsorbate surface interactions: While experiments used *cis*-OA as the QD ligand, here we modeled the adsorption of a shorter chain carboxylic acid (specifically, 4-heptenoic acid) to better understand how the carboxylic acid could interact with the NP surface. The carboxylic acid ligands and the 2 × 2 × 3 CdS surface are depicted in Fig. S11 and S12,† respectively. We investigated multiple configurations including two vertical orientations where either (a) the carboxylic acid (COOH) end or (b) the alkyl (CH_3) end was interacting with the surface, another vertical orientation where (c) the carboxylic acid was deprotonated (COO^-/H^+), and finally (d) a horizontal orientation (flat) to gauge the strength of the alkene double bond on the surface. The relaxed structures of these four configurations are depicted in Fig. 6. Our adsorp-

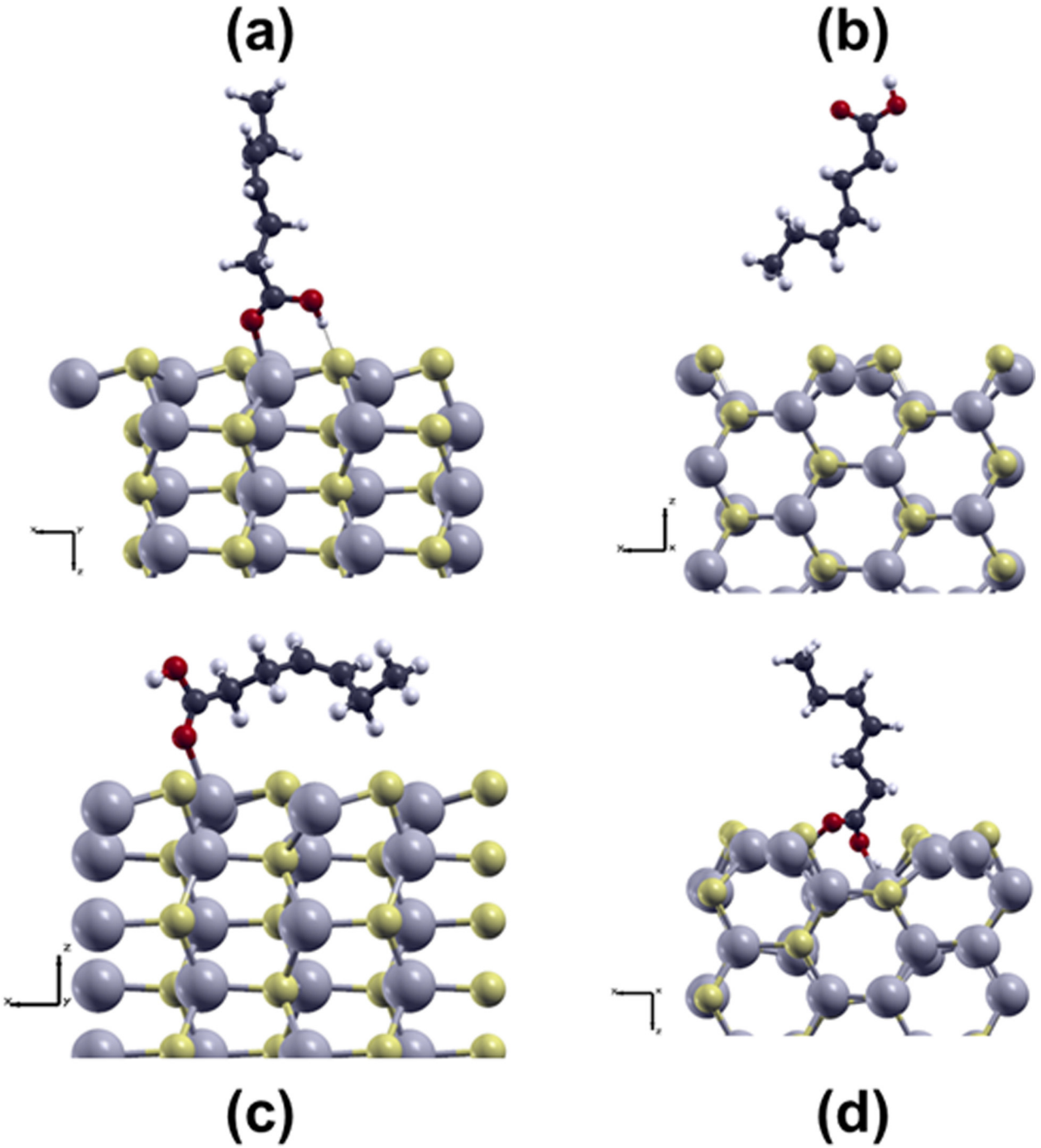

Fig. 6 Depiction of the final adsorption geometries for a single *cis* isomer of 4-heptenoic acid with the (a) COOH or (b) CH_3 group pointed towards the CdS surface, the (c) flat configuration, and (d) the COO^-/H^+ starting structure, where H^+ migrates back towards the COO^-, reattaching itself to complete the COOH unit. Cd atoms are illustrated here as gray spheres, S atoms as yellow spheres, O atoms as red spheres, C atoms as black spheres, and H atoms as white spheres.

Table 2 Adsorption energies (E_{ads}) for the four single adsorption configurations of 4-heptenoic acid on the 2 × 2 × 3 CdS surface, in both the *cis* and *trans* configurations

cis	E_{ads} (eV)	E_{ads} (kcal mol^{-1})	*trans*	E_{ads} (eV)	E_{ads} (kcal mol^{-1})
COOH	−0.607	−13.998	COOH	−0.612	−14.115
Flat	−0.456	−10.509	Flat	−0.456	−10.526
CH_3	−0.019	−0.435	CH_3	−0.038	−0.866
COO^- [a]/H^+	−0.390	−9.000	COO^- [a]/H^+	−0.297	−6.838

[a] The COO^- geometries only appear favorable because re-protonation occurs, allowing the structure to revert to a similar geometry as the COOH configuration.

tion energy (E_{ads}) findings on the 2 × 2 × 3 CdS surface are reported in Table 2. Also tabulated in Table 2 are the E_{ads} for the same configurations of the *trans* isomer of 4-heptenoic acid on CdS. The *trans* isomer was included to discern whether changes in the stereochemistry of the ligand affect adsorption energy and/or geometry. The similarities shown imply these results could be applicable to different isomers of OA. The trend in E_{ads} for both the *cis* and *trans* isomers is that COOH > flat > CH_3 > COO^-/H^+. Our interpretation of this trend is that it is energetically favorable for an alkane to weakly interact with the CdS surface, but less favorable than when a double bond is present, either as an alkene or carboxylic acid.

Although the *cis* and *trans* configurations have similar adsorption energies, these energies are markedly different for the dimeric configurations with changes in orientation. The range of −1.244 to −0.115 eV for the different changes in orientation show that reorganization differences can be up to 0.6 eV per adsorbate, which is approximately 30× kT.

Table S1† tabulates the same E_{ads} for adsorbates on a 3 × 3 × 3 CdS surface to assess whether the trends in relaxed geometry and E_{ads} are comparable on larger more extended surface systems. The trend in E_{ads} for both the *cis* and *trans* isomers on the 3 × 3 × 3 CdS surface was also COOH > flat > CH_3 > COO^-/H^+, however, on the larger 3 × 3 × 3 surface, we found that the COO^-/H^+ configuration was not stable for either the *cis* or *trans* isomer of 4-heptenoic acid. The COO^- and H^+ groups were further separated than on the 2 × 2 × 3 CdS surface and we believe that the tendency for the COO^-/H^+ to reprotonate is related to the separation distance of COO^- and H^+, which here is dictated by the in-plane dimensions of the surface slab.

While there is a predicted order in which the adsorption energies of these ligands increase, it is important to note that all of them are still negative, representing a favorable interaction. What changes to a varying degree is the favorability of different surface–ligand geometries, *i.e.*, the more negative adsorption energy values are more likely to occur, however all interactions with a negative adsorption energy could occur.

We found large changes in the adsorbate geometry optimization of the flat and COO^-/H^+ configurations from the initial to final relaxed coordinates for both the 2 × 2 × 3 and 3 × 3 × 3 surfaces. In the flat orientation, the alkene bond is pushed anywhere from 2.78 to 7.58 Å away from the CdS surface, relative to the starting geometry, allowing the surface to interact more with the carboxylic end of the adsorbate than the alkane end. The favorable interactions form at least one Cd–O bond per relaxed structure. This is also observed for the fully relaxed COO^-/H^+ configuration on the 2 × 2 × 3 surface, where the H^+ migrates back towards the COO^-, reattaching itself to complete the COOH unit, and then forming a Cd–O bond. This migration does not occur on the 3 × 3 × 3 surface; the COO^- and H^+ are separated by more than 3 Å.

The range of E_{ads} computed for the *cis* isomer interacting with the 2 × 2 × 3 CdS surface in the COOH, flat, and COO^-/H^+ structures is −0.390 to −0.607 eV, while the CH_3 structure is −0.019 eV, which is not as favorable an E_{ads}. Single adsorbate geometry relaxations result in Cd–O bond distances of approximately 2.35 ± 0.03 Å, while the –OH forms hydrogen bonds with S terminations at distances of approximately 2.00 ± 0.1 Å. The full range of DFT-computed surface Cd-interaction distances is listed in Table 3 and includes monomer, dimer, and hexamer values. The distance of the *cis* isomer vertical ligands to the surface was measured from both the H and C of the vertical ligand to the nearest surface Cd and S, and an example of these values from the monomer can be seen in Table 4. These distances are shown to decrease from the monomer to the hexamer system, implying that these ligands are stabilized closer to the surface by neighboring ligands. Depictions of which measurements were made, as well as specific distance values for the dimer and hexamer systems, can be found in Fig. S13–S15 and Tables S2, S3.†

(b) Multiple adsorbate surface interactions: Configurations with either two adsorbates (referred to as dimers) or six adsorbates (referred to as hexamers) placed together on the 2 × 2 × 3 CdS surface were modeled to uncover pairwise interactions that could result from multiple geometry and ligand orientation changes. Due to the reduced favorability of the COO^-/H^+ charge-separated configurations on the 2 × 2 × 3 and 3 × 3 × 3 CdS surfaces, this configuration was not included in the dimer and hexamer calculations. Neither was the flat configuration, as dimer pairs took up too much horizontal space on the CdS surface. The orientations investigated here included (i) both alkyl groups facing the surface, (ii) both carboxylic groups facing the surface, and (iii) alternating functional groups facing the surface; these three configurations are shown in Fig. 7. The two most energetically favorable conformations of this set (based on data shown in Table 5) were then also tested with three pairs on a single surface, for a total of six ligand

Table 3 The full range of interaction distances, in units of Å, of each of the 4-heptenoic acid adsorbate configurations with their nearest Cd neighbor

Interaction	Distance (Å)
Cd–O	2.320–2.380
S–H	1.910–2.095
Vertical	3.134–5.514
Flat (with Cd–O)	7.295–7.577
Flat (without Cd–O)	**2.779–2.821**

Table 4 A sampling of distances from the closest H and end C on the alkyl chain of the vertical monomer ligand to the closest Cd and closest S on the surface. All distances are in units of Å

Atoms measured	Distance (Å)
C : Cd	5.513
C : S	4.814
H1 : Cd	5.033
H2 : Cd	5.324
H1 : S	4.844
H2 : S	4.354

Table 5 Adsorption energies (E_{ads}) for the three *cis* isomer dimeric adsorption configurations on the 2 × 2 × 3 CdS surface. Given the results of the single adsorbate studies, these were not replicated on the 3 × 3 × 3 surface. Results of the *trans* isomer ligand adsorptions can be found in the ESI Table S4†

Configuration	E_{ads} (eV)	E_{ads} (kcal mol^{-1})
2 × COOH	−1.244	−28.696
COOH + CH_3 alt.	−0.691	−15.928
2 × CH_3	−0.115	−2.666

adsorbates. This was modeled due to the relatively high concentrations of adsorbates present in the laboratory experiment. Here our ligands are modeled in doubles for computational convenience to better understand the pairwise ligand interactions that could occur at the surface of CdS. We view this 50% OA flip as the minimum fraction that could occur in the basic water experiments described in the previous section. Bond lengths in the dimer and hexamer configurations were consistent with the values found in the single adsorbate studies that are reported in Tables 3 and 4.

Dimer pair adsorption energies on the fully relaxed 2 × 2 × 3 CdS surfaces were found to align closely with those of the individual adsorbates; each COOH interaction was approximately −0.6 eV and each CH_3 was approximately 0.5 eV higher in energy; the E_{ads} of all three configurations are shown in Table 5. The hexamer systems, however, relaxed to energies lower than the sum of individual adsorbates in the system. Favorable hydrogen–sulfur (H–S) bonding interactions with the surface stabilize the adsorbates with –COOH facing the surface (O–H–S), as does the formation of strong Cd–O bonds. When half of the hexamers are reoriented such that three CH_3 groups are pointed at the surface, creating COOH/CH_3 dimeric pairs, the COOH of those reoriented molecules form a hydrogen bonding network above the ligand set that was not previously observed when all COOH pointed towards the surface. Both interactions can be seen in Fig. 8 and their E_{ads} are tabulated in Table 6. In addition, the adsorption energy of a ligand pair of opposite alignment, and with opposite stereochemistry, yields an E_{ads} between that of the *cis* and the *trans* isomer pairs with the same alignment, implying that stereochemistry is not as important as spatial orientation when estimating E_{ads}.

Additional ligands lead to lower adsorption energies, possibly due to H-bonding interactions among them. However, this effect does not decrease linearly, as the dimer pair energy is not double the energy of the single ligand. Notably, the energy difference between the dense carboxylic oriented hexamer surface and the oppositely oriented hexamer surface is very small, implying that both configurations could be stable on the surface. In other words, 50% of the ligands could flip to create a hydrogen bonding network and still have a favorable E_{ads} as there is an additional stabilization effect that arises from dense ligand packing at the surface. Fig. 8 shows that

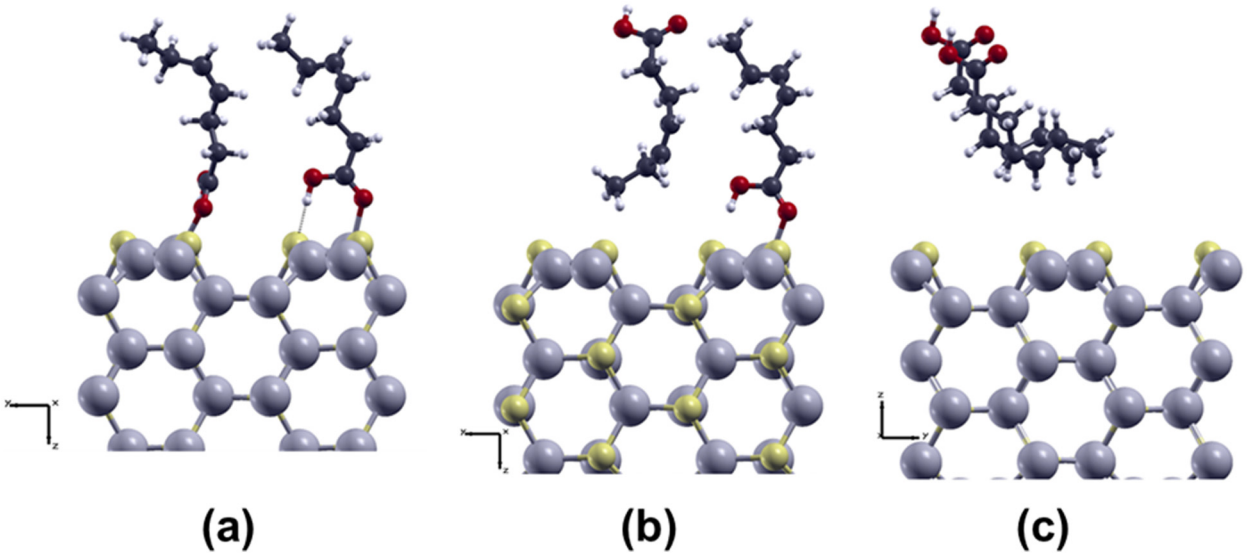

Fig. 7 Depiction of the final adsorption geometries for a dimer pairing of the *cis* isomer ligand with (a) both COOH groups pointed toward the surface, (b) one COOH and one CH_3 group alternating, and (c) both CH_3 groups pointed towards the surface. Cd atoms are illustrated here as gray spheres, S atoms as yellow spheres, O atoms as red spheres, C atoms as black spheres, and H atoms as white spheres.

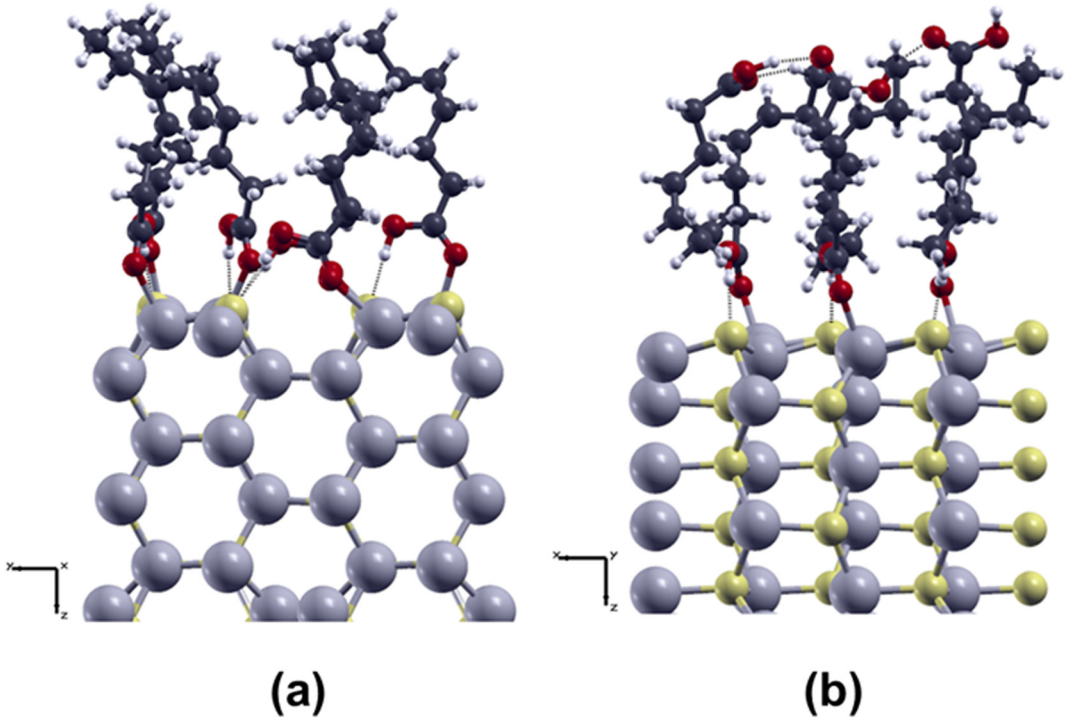

Fig. 8 Depiction of the final adsorption geometries for two hexamer configurations of the *cis* isomer ligand with (a) all six COOH groups pointed toward the surface, and (b) three COOH groups pointed towards the surface and three CH_3 groups pointed towards the surface. The adsorption energies of these systems are lower than the sum of the individual adsorbates that comprise them, indicating that both are predicted to be favorable motifs. Cd atoms are illustrated here as gray spheres, S atoms as yellow spheres, O atoms as red spheres, C atoms as black spheres, and H atoms as white spheres. Figure (a) is viewed down the *x*-axis, while figure (b) is viewed down the *y*-axis. Another angle is shown in Fig. S15.†

Table 6 Adsorption energies (E_{ads}) for three *cis*-dimer pairs (hexamer) adsorption configurations on the 2 × 2 × 3 CdS surface depicted in Fig. 8. Notably, each of these configurations yields an adsorption energy lower than the sum of the individual adsorbates. Results of the *trans* ligands can be found in the ESI Table S5†

Configuration	E_{ads} (eV)	E_{ads} (kcal mol^{-1})
COOH × 6	−3.399	−78.394
(COOH + CH_3) × 3	−2.507	−57.820

there are hydrogen bonding interactions that stabilize the oppositely aligned pairs (seen in detail in Fig. S15†). This opposing alignment exposes polar carboxylic groups to the solvent, which could explain the solubility of the OA-capped NPs in a polar solvent such as water. Moreover, the configurations shown in Fig. 8 are very similar in energy despite the left one having three fewer Cd–O bonding adsorbates than the right. The results appear to indicate that the adsorption energies on full NP surfaces will be very similar for configurations where all of the COOH groups face the surface and where half of the COOH groups face the solvent, in alternating pairs. The additional energy reduction due to solvation of the COOH groups in aqueous media will most likely mean that the reorientation of ligands to form oppositely-ordered pairs is favored.

Conclusions

In summary, this study describes a simple, single-step method to transfer OA-capped hydrophobic NPs into water-based environments: the NPs studied here are CdSe/CdS QDs and magnetite NPs. Red-emitting QDs synthesized in hexane were transferred into basic water within 4 h at room temperature without requiring any extra reagents. The water solubilization process was found to be pH-dependent, and the best outcome was achieved in alkaline medium (pH 8). We propose that the transfer of QDs in water is enabled by the rearrangement of the OA ligands at the surface of the particles to form a "mixed" monolayer, where part of the carboxylic acid moieties stay attached to the surface of the QDs while the carboxylic acid moieties of the remaining OA ligands are directed towards the aqueous media. This hypothesis is supported by DFT studies, which provide evidence that when 50% of the ligands are flipped, the interactions will be energetically favorable in aqueous media.

Transfer of QDs into water was accompanied by an unusual increase in their photoluminescence quantum yield. Future directions will include the extension of this technique to a wider variety of OA-capped NPs as well as NPs capped with other molecules that might also favor the formation of "mixed" monolayers. DFT calculations may be extended to include solvation effects, larger surfaces with more dimer

pairs, as well as explorations of other surfaces based on the wurtzite structure type to better understand the relationship between surface atom identity, orientation, and the strength of carboxylic acid adsorption.

We expect that our findings will open broad opportunities for NPs synthesized in organic solvents to be used in water-based applications. For instance, these QDs could be used in biomedical research since we have demonstrated their stability in physiological buffers, remaining colloidally stable for over one week in 0.1× PBS and more than 12 hours in 1× PBS. In addition, these QDs are well suited for photonic applications requiring dispersion in aqueous media, such as systems involving metal NPs, which are typically prepared in water. In such hybrid assemblies, the enhanced PLQY achieved through this method can improve optical performance, offering potential benefits for sensing and detection platforms. These QD–metal NP assemblies can also be applied in environmental monitoring and analyte detection, where enhanced sensitivity is essential.[40] The aqueous compatibility and stable optical properties of these QDs are consistent with current advancements in the field, where QDs are increasingly recognized for their role in sensitive fluorescence-based detection of pollutants.[41–43] Furthermore, the presence of surface-exposed carboxyl groups provides reactive sites for binding target analytes like heavy metal ions. These characteristics make them promising candidates for the development of optical sensors for environmental monitoring applications.

Experimental section

Chemicals

To prepare QDs, cadmium oxide (CdO, ≥99.99%, Sigma Aldrich, St Louis, MO, USA), selenium powder 100 mesh (Se, 99.99%, Sigma Aldrich), sulfur (S, ≥99.5%, Acros), trioctylphosphine (TOP, 97%, Aldrich), oleic acid (OA, >97%, Fisher Science Education), oleylamine (primary amine >98%, Sigma Aldrich), 1-octadecene (90%, Sigma Aldrich), hexadecylamine (98%, Sigma Aldrich), hexane (Thermo Fisher Scientific, Waltham, MA, USA), methanol (Thermo Fisher Scientific) and acetonitrile (Pharmco-AAPER, Brookfield, CT, USA) were used as received. To prepare magnetite NPs, $FeCl_2{\cdot}4H_2O$ (≥99%, Sigma Aldrich), sodium hydroxide (NaOH, ≥98%, Sigma Aldrich), hydrochloric acid (HCl, 36%, Thermo Fisher Scientific), and acetone (Thermo Fisher Scientific) were used as received. All heating procedures were carried out using heating mantles.

Synthesis of CdSe/CdS QDs

The synthesis of red-emitting CdSe QDs is based on a modified version of the procedure used by Zhong *et al.*[44] In brief, 0.1658 g of Se powder was dissolved into 1 mL of TOP in a small 25 mL round bottom flask equipped with a stir bar to prepare the Se precursor for the reaction. The Se solution turned black after vortexing. In order to prepare the Cd precursor solution, 0.3852 g of CdO was mixed with 5 mL of OA and 5 mL of 1-octadecene in another small round bottom flask and the resulting solution was heated to 250 °C under inert nitrogen gas. After the dissolution of the CdO powder, the reaction temperature was decreased to 60 °C while stirring and keeping under inert atmosphere. The Cd precursor solution was translucent but not colorless.

In a 3-neck round bottom flask, 0.15 mL of the Se precursor was mixed with 5 mL of oleylamine and heated to 90 °C for 20 minutes under N_2 atmosphere to degas the reaction mixture. Afterward, the reaction temperature was increased to 300 °C and, upon reaching this temperature, 1 mL of the Cd precursor was injected using a degassed glass syringe. A rapid formation of gas was an indication of the reaction proceeding. Small aliquots (50 to 100 μL) of the resulting mixture were diluted with 2 mL toluene and were analyzed by UV-Vis spectroscopy 5 min, 10 min, 15 min, 20 min, 30 min and 60 min after injection of the Cd precursor. The reaction was stopped by removing the heat source once the desired first exciton peak at around 625 nm was reached and there was no more change in the peak position.

The purification of CdSe QDs was performed through a methanol/hexane extraction. To accomplish this, further hexane needs to be added to the methanol/hexane mixture (*e.g.*, around 150 mL methanol/250 mL hexane) until it results in easy separation of two liquid phases. The extraction was carried out three times (using 100–150 mL methanol each time) and the hexane layer was concentrated under reduced pressure. The solvent was not completely evaporated, and the purified QDs were kept in a few mL of hexane for the next step.

To modify the surface of CdSe QDs with a CdS shell, the SILAR method was followed by adapting the protocols of Xie *et al.*[37] and Li *et al.*[38] In brief, 1.5 mL of 1-octadecene and 0.5 g of hexadecylamine were added to the purified CdSe QDs in a 3-neck round bottom flask. The reaction proceeded under N_2 atmosphere by stirring for 30 min at 100 °C, then heating to 235 °C. Two precursor solutions were prepared: a sulfur and a cadmium precursor. Both precursors were kept under N_2 gas in small round bottom flasks. To prepare the sulfur precursor, 0.032 g of sulfur powder was dissolved in 10 mL octadecene by heating to 180 °C under stirring and the solution was then kept at room temperature. The Cd precursor of the CdS shell was prepared by the addition of 0.3204 g of CdO to 7 mL of OA and 18 mL of octadecene. The mixture was heated to 240 °C, followed by cooling down to 80 °C. Nine layers of CdS shell were formed onto the surface of the CdSe QD cores through alternating addition of the two precursor solutions at 10 min intervals. In accordance with Table S6,† different amounts of precursors were injected into CdSe QDs solutions at 235 °C for different layers formation. Each layer was formed by adding Cd precursor to the solution, followed by 10 min stirring, then adding the sulfur precursor followed by another 10 min stirring.

The resulting CdSe/CdS QDs had a size of approximately 13 nm (measured using TEM), a first exciton absorbance at 644 nm, and an emission wavelength of 657 nm.

For the synthesis of the second batch of CdSe/CdS QDs with higher PLQY, a different protocol for the shell growth was followed. The modified Zhong *et al.* method described above

was maintained for the CdSe core synthesis. Also, the CdSe cores were purified likewise, as described above. However, the Hanifi *et al.*[39] method was adapted to grow the CdS shell around 125 nanomoles of CdSe cores. The CdS shell growth began with the preparation of cadmium oleate. A 0.2 M solution was prepared by combining 0.514 g of cadmium oxide with 12.62 mL of OA (1 : 10 molar ratio) and 7.32 mL of 1-octadecene in a 50 mL Schlenk flask fitted with a rubber septum and thermocouple adapter and connected to a Schlenk line. The solution was degassed at 110 °C for two hours and then heated to 160 °C under nitrogen gas until the cadmium complexation was complete, which took one hour. Afterward, the reaction was cooled to 110 °C and degassed for two hours. In parallel, the sulfur precursor was prepared by mixing 0.7 mL of 1-octanethiol with 19.3 mL of 1-octadecene at room temperature under nitrogen gas. For the CdS shell growth, 6 mL of 1-octadecene was degassed for one hour at 110 °C in a 50 mL Schlenk flask, fitted with a rubber septum and thermocouple adapter, and connected to a Schlenk line. After that, the CdSe QD cores were added, and hexane was removed under vacuum. After the reaction mixture was hexane-free, the temperature was raised to 240 °C, and 14.68 mL of cadmium precursor and sulfur precursor respectively were simultaneously injected using a dual syringe pump at a 3 mL per hour rate. Once started, the temperature was raised to 310 °C and maintained for the entire duration of the shell growth. The reaction continued for 10 minutes after the injection was complete before cooling to ambient temperature. The final CdSe/CdS QDs were 12 nm in diameter, with a first exciton absorbance at 644 nm and an emission wavelength of 661 nm.

Synthesis of magnetite NPs

The procedure for the preparation of OA-coated magnetite (Fe_3O_4) NPs was carried out by following the protocol reported by Patil *et al.*[45] In a round bottom flask, 2 g of $FeCl_2{\cdot}4H_2O$ was added to 20 mL HCl (2 M) and the mixture was heated to 70 °C under stirring. Then, 25 mL of 3 M NaOH was added dropwise to the resulting solution while stirring. A black precipitate formed, and this precipitate was washed several times with distilled water to reach neutral pH. Magnetic separation was applied for washing purposes and, finally, the precipitate was dried in an oven at 100 °C for 3 h. To modify the surface of magnetite NPs with OA ligands, 1 g of unmodified magnetite NPs was suspended in 100 mL of methanol in a round bottom flask and this solution was stirred and heated in an oil bath at 80 °C. To the resulting mixture, 10 mL of OA was added dropwise, and the reaction was heated for several hours while stirring at 80 °C until all solvent was evaporated. The modified magnetite NPs were washed several times with distilled water and acetone to remove the excess amount of OA. The final product was recovered using a magnet and obtained by drying at 50 °C in the oven for about 6 h.

Transfer of NPs from hexane to aqueous media

The crude CdSe/CdS QDs (1 mL) were diluted with 10 mL of hexane and were extracted against 25 mL of methanol (at least five times). 1 mL of washed diluted QDs with absorbance about 0.1 at 644 nm was mixed with 0.5 mL acetonitrile in order to obtain a higher isolation yield. The mass of QDs in a 1 mL sample was about 1.5 mg. The resulting mixture was centrifuged at 21 000*g* for 30 min at 7 °C to get a pellet, then the supernatant was removed with a micropipette. Approximately 5 μL of solvent was left with the pellet. At this step, the resulting pellet was redispersed in water media (1 mL of pH 8 solution, using KOH, or pH 6 Millipore water) and a very cloudy solution was initially seen in the centrifuge tube. The solution was sonicated at room temperature for 2 minutes at one-hour intervals over a total period of 4 hours (*i.e.* a total of four 2 min sonications), and was then left undisturbed overnight at room temperature.

For magnetite NPs, the powder of OA-coated Fe_3O_4 NPs (2 mg) was directly suspended in water or hexane (4 mL) using sonication, and dispersion behaviors were investigated as a function of time.

Characterization and sonication equipment

Sonication was carried out using a Fisherbrand CPX digital ultrasonic bath (1.9 L) from Fisher Scientific. A Beckman DU730 UV-Vis spectrophotometer (Beckman, Brea, CA, USA) was used for the absorption analyses of QDs samples in different media. PL measurements were carried out using a DUETTA fluorometer (Horiba, Piscataway, NJ, USA); the excitation wavelength was adjusted to 470 nm. To image QDs, transmission electron microscopy (TEM, Hitachi 7800, Santa Clara, CA, USA) was utilized. The Fourier transform infrared (FT-IR) spectra were recorded using a PerkinElmer Frontier Optica FT-IR instrument (Shelton, CT, USA) and the Nuclear Magnetic Resonance (NMR) spectra were obtained using a JEOL 400 MHz spectrometer (Tokyo, Japan). The solutions were also analyzed using Dynamic Light Scattering (DLS) with the Zetasizer Nano-ZS system (Malvern Instruments, Southborough, MA, USA).

Simulation of QD system using open-source computational packages

(a) Adsorbate modeling: Due to computational limitations, the full 18 carbon chain of OA was substituted with 4-heptenoic acid as it contains both alkene and carboxylic acid functional groups and is the closest location for the double bond to avoid possible conjugation interactions or cyclizations with the carboxylic acid. Modeling efforts employed both the *cis*- and *trans*-isomer for surface adsorbate relaxations. Each adsorbate was also tested in four different orientations against the CdS surface. Fig. S11† shows the two isomeric configurations of the adsorbate.

(b) Surface model generation: The CdS surfaces employed here are intended to be an approximated localized model of a core–shell CdSe/CdS QD surface. Previous studies[46] determined that the (101) surface termination was the most stable cleavage plane of CdS surfaces. CrystalMaker®[47] was used to generate CdS (101) surfaces of dimension 2 × 2 × 3 and 3 × 3 × 3 unit cells, which terminated in alternating cadmium and sulfur atoms. They contained 96 and 216 atoms, respectively. After a full geometry optimization and atomistic relaxation, the

Cd–S bonds in the surface are between 2.51–2.56 Å and the S–Cd–S bond angles are between 105–114°. Three different views of the CdS (101 or 112-bar0) surface are shown in Fig. S12.† These surfaces were placed in close contact with single adsorbates and multiple configurations that contained two to six adsorbates.

(c) Computational parameters: We employed Quantum ESPRESSO,[48,49] an open-source plane-wave DFT software package, for all calculations. Each atom was represented using GBRV-type ultrasoft pseudopotentials.[50,51] A plane-wave cutoff of 40 Ry and charge density cutoff of 320 Ry were used for all calculations, in line with similar surface studies.[52,53] Adsorbate geometry optimizations were obtained using a box 20 Å per side. Bulk structural relaxations of CdS used a 4 × 4 × 4 *k*-point grid[54] and then a 2 × 2 × 1 *k*-point grid for adsorbate–surface systems, which included 15 Å of vacuum. The energy convergence criteria for self-consistent relaxations was 5×10^{-6} eV. Geometry optimization of all surface–adsorbate interactions did not include fixing any layers, so all atoms were allowed to fully relax.[55] All calculations were performed at the General Gradient Approximation (GGA) level using the Wu-Cohen (WC) modified PBE-GGA exchange correlation functional for solids.[56,57] All figures were generated using XCrysDen,[58] an open-source molecular structure visualization software package.

The adsorption energy (E_{ads}) is calculated by subtracting the sum of the initial surface and adsorbate energy from the final energy of the total system, illustrated in eqn (1). From right to left, $E_{adsorbate}$ is the energy of the adsorbate (alone in a box of length 20 Å), $E_{surface}$ is the energy of the supercell slab structure (2 × 2 × 3 or 3 × 3 × 3), and E_{sys} is the final energy of the relaxed surface–adsorbate structure. The result of this calculation is E_{ads}, the total energy of the interaction of the adsorbate with the surface.

$$E_{ads} = E_{sys} - (E_{surface} + E_{adsorbate}) \quad (1)$$

Author contributions

T. B. K. conducted experiments and measurements for the project, analyzed data, and drafted the manuscript. J. T. performed computational studies for the project, analyzed data, and contributed to writing the manuscript. C. M. L. and L. A. contributed to the synthesis of QDs batches and created the artwork. M. P. applied his expertise to analyze data and contributed to editing the manuscript. J. W. B. supervised the computational part of the project, analyzed data, and contributed to editing the manuscript. M. C. D. supervised the research project, analyzed data, and contributed to editing the manuscript.

Data availability

The data supporting this article have been included as part of the ESI.†

Conflicts of interest

The authors have no conflict of interest to declare.

Acknowledgements

The authors are grateful to the U.S. National Science Foundation (DMR-1905135) for financial support of the work on magnetite NPs as well as some of the work on QDs. Synthesis and characterization of the QDs was also partially supported by the U.S. National Science Foundation Science and Technology Center (STC) for Integration of Modern Optoelectronic Materials on Demand (IMOD) under Cooperative Agreement No. DMR-2019444. The computational work used the Extreme Science and Engineering Discovery Environment (XSEDE),[59] which is supported by the U.S. National Science Foundation grant number ACI-1548562 through allocation ID TG-CHE200108. The authors would like to thank Dr Tagide de Carvalho (Keith R. Porter Imaging Facilities, UMBC) for her help with TEM imaging. Furthermore, they wish to express their gratitude to Dr Marcin Ptaszek and Brandon Busick for performing the PLQY measurements and to Elizabeth Kane for the single-QD PL measurements.

References

1 V. I. Klimov, A. A. Mikhailovsky, S. Xu, A. Malko, J. A. Hollingsworth, C. A. Leatherdale, H. J. Eisler and M. G. Bawendi, *Science*, 2000, **290**, 314–317.
2 D. J. Norris and M. G. Bawendi, *Phys. Rev. B: Condens. Matter Mater. Phys.*, 1996, **53**, 16338–16346.
3 M. A. Cotta, *ACS Appl. Nano Mater.*, 2020, **3**, 4920–4924.
4 M. M. Barroso, *J. Histochem. Cytochem.*, 2011, **59**, 237–251.
5 X. H. Gao, L. L. Yang, J. A. Petros, F. F. Marshal, J. W. Simons and S. M. Nie, *Curr. Opin. Biotechnol.*, 2005, **16**, 63–72.
6 O. Chen, J. Zhao, V. P. Chauhan, J. Cui, C. Wong, D. K. Harris, H. Wei, H. S. Han, D. Fukumura, R. K. Jain and M. G. Bawendi, *Nat. Mater.*, 2013, **12**, 445–451.
7 S. S. Wang, Y. R. Wen, Y. J. Wang, Y. Y. Ma and Z. Liu, *Anal. Chem.*, 2017, **89**, 5646–5652.
8 J. Kim, S. Song, Y. H. Kim and S. K. Park, *Small Struct.*, 2021, **2**, 2000024.
9 J. Zhang, S. Zhang, Y. Zhang, O. A. Al-Hartomy, S. Wageh, A. G. Al-Sehemi, Y. Hao, L. Gao, H. Wang and H. Zhang, *Laser Photonics Rev.*, 2023, **17**, 2200551.
10 A. P. Litvin, I. V. Martynenko, F. Purcell-Milton, A. V. Baranov, A. V. Fedorov and Y. K. Gun'ko, *J. Mater. Chem. A*, 2017, **5**, 13252–13275.
11 D. Harankahage, J. Cassidy, M. R. Yang, D. Porotnikov, M. Williams, N. Kholmicheva and M. Zamkov, *J. Phys. Chem. C*, 2021, **125**, 22195–22203.

12 P. Yang, M. Ando and N. Murase, *Langmuir*, 2011, **27**, 9535–9540.
13 A. M. Derfus, W. C. W. Chan and S. N. Bhatia, *Nano Lett.*, 2004, **4**, 11–18.
14 J. S. Chen, B. Yang, C. S. Li, K. B. Zheng, K. Zidek and T. Pullerits, *ACS Omega*, 2017, **2**, 1922–1929.
15 E. Petryayeva, W. R. Algar and I. L. Medintz, *Appl. Spectrosc.*, 2013, **67**, 215–252.
16 W. W. Yu, E. Chang, R. Drezek and V. L. Colvin, *Biochem. Biophys. Res. Commun.*, 2006, **348**, 781–786.
17 N. N. Wei, L. Li, H. G. Zhang, W. F. Wang, C. J. Pan, S. D. Qi, H. Y. Zhang, H. L. Chen and X. G. Chen, *Langmuir*, 2019, **35**, 4806–4812.
18 W. Z. Guo, J. J. Li, Y. A. Wang and X. G. Peng, *Chem. Mater.*, 2003, **15**, 3125–3133.
19 K. Susumu, H. T. Uyeda, I. L. Medintz, T. Pons, J. B. Delehanty and H. Mattoussi, *J. Am. Chem. Soc.*, 2007, **129**, 13987–13996.
20 Y. F. Ma, Y. Li, S. J. Ma and X. H. Zhong, *J. Mater. Chem. B*, 2014, **2**, 5043–5051.
21 X. H. Pham, S. M. Park, K. M. Ham, S. Kyeong, B. S. Son, J. Kim, E. Hahm, Y. H. Kim, S. Bock, W. Kim, S. Jung, S. Oh, S. H. Lee, D. Hwang and B. H. Jun, *Int. J. Mol. Sci.*, 2021, **22**, 10116.
22 D. Janczewski, N. Tomczak, M. Y. Han and G. J. Vancso, *Nat. Protoc.*, 2011, **6**, 1546–1553.
23 N. Tomczak, R. R. Liu and J. G. Vancso, *Nanoscale*, 2013, **5**, 12018–12032.
24 A. Prakash, H. G. Zhu, C. J. Jones, D. N. Benoit, A. Z. Ellsworth, E. L. Bryant and V. L. Colvin, *ACS Nano*, 2009, **3**, 2139–2146.
25 J. C. K. Alexander, M. Saeboe, and A. M. Dennis, in *Quantum Dots: Applications in Biology, Methods in Molecular Biology*, ed. A. F. A. B. S. Santos, Springer Science+Business Media, LLC, part of Springer Nature, New York, 2020, vol. 2135, ch. 5, pp. 95–108.
26 L. Gomez, C. de Weerd, J. L. Hueso and T. Gregorkiewicz, *Nanoscale*, 2017, **9**, 631–636.
27 Y. Y. Fan, H. L. Liu, R. C. Han, L. Huang, H. Shi, Y. L. Sha and Y. Q. Jiang, *Sci. Rep.*, 2015, **5**, 9908.
28 K. Suga, D. Kondo, Y. Otsuka, Y. Okamoto and H. Umakoshi, *Langmuir*, 2016, **32**, 7606–7612.
29 G. E. Dobretsov, T. I. Syrejschikova and N. V. Smolina, *Biophysics*, 2014, **59**, 183–188.
30 J. Maillard, K. Klehs, C. Rumble, E. Vauthey, M. Heilemann and A. Furstenberg, *Chem. Sci.*, 2021, **12**, 1352–1362.
31 J. X. Xu, F. Y. Yan, X. D. Sun and Z. X. Wang, *J. Photochem. Photobiol., A*, 2019, **382**, 111938.
32 B. Zeng, G. Palui, C. Zhang, N. Zhan, W. Wang, X. Ji, B. Chen and H. Mattoussi, *Chem. Mater.*, 2018, **30**, 225–238.
33 Z. Hens and J. C. Martins, *Chem. Mater.*, 2013, **25**, 1211–1221.
34 B. Fritzinger, R. K. Capek, K. Lambert, J. C. Martins and Z. Hens, *J. Am. Chem. Soc.*, 2010, **132**, 10195–10201.
35 M. J. Hostetler, J. E. Wingate, C.-J. Zhong, J. E. Harris, R. W. Vachet, M. R. Clark, J. D. Londono, S. J. Green, J. J. Stokes, G. D. Wignall, G. L. Glish, M. D. Porter, N. D. Evans and R. W. Murray, *Langmuir*, 1998, **14**, 17–30.
36 Y. Tao, Z. Tang, D. Bao, H. Zhao, Z. Gao, M. Peng, H. Zhang, K. Wang and X. Sun, *Small*, 2023, **19**, 2206316.
37 R. G. Xie, U. Kolb, J. X. Li, T. Basche and A. Mews, *J. Am. Chem. Soc.*, 2005, **127**, 7480–7488.
38 J. J. Li, Y. A. Wang, W. Z. Guo, J. C. Keay, T. D. Mishima, M. B. Johnson and X. G. Peng, *J. Am. Chem. Soc.*, 2003, **125**, 12567–12575.
39 D. A. Hanifi, N. D. Bronstein, B. A. Koscher, Z. Nett, J. K. Swabeck, K. Takano, A. M. Schwartzberg, L. Maserati, K. Vandewal, Y. van de Burgt, A. Salleo and A. P. Alivisatos, *Science*, 2019, **363**, 1199–1202.
40 P. Malik, J. Singh and R. Kakkar, *Adv. Mater. Lett.*, 2014, **5**, 612–628.
41 P. Gupta, G. Tamrakar, S. Biswas, R. S. Dhundhe, V. K. Soni, H. S. Das, P. Sahu, A. K. Chaturwedi, N. K. Kashyap, T. Akitsu and M. Hait, *ES Chem. Sustainability*, 2024, **1**, 1359.
42 D. Wang, F. Gao, X. Wang, X. Ning, K. Wang, X. Wang, Y. Wei and T. Fujita, *Toxics*, 2022, **10**, 367.
43 Y. Lou, Y. Zhao, J. Chen and J.-J. Zhu, *J. Mater. Chem. C*, 2014, **2**, 595–613.
44 X. H. Zhong, Y. Y. Feng and Y. L. Zhang, *J. Phys. Chem. C*, 2007, **111**, 526–531.
45 R. M. Patil, P. B. Shete, N. D. Thorat, S. V. Otari, K. C. Barick, A. Prasad, R. S. Ningthoujam, B. M. Tiwale and S. H. Pawar, *RSC Adv.*, 2014, **4**, 4515–4522.
46 S. Hamad, S. Cristol and C. R. A. Callow, *J. Phys. Chem. B*, 2002, **106**, 11002–11008.
47 D. C. Palmer, *CrystalMaker*, CrystalMaker Software Ltd, Begbroke, Oxfordshire, England, 2014.
48 P. Giannozzi, S. Baroni, N. Bonini, M. Calandra, R. Car, C. Cavazzoni, D. Ceresoli, G. L. Chiarotti, M. Cococcioni, I. Dabo, A. Dal Corso, S. de Gironcoli, S. Fabris, G. Fratesi, R. Gebauer, U. Gerstmann, C. Gougoussis, A. Kokalj, M. Lazzeri, L. Martin-Samos, N. Marzari, F. Mauri, R. Mazzarello, S. Paolini, A. Pasquarello, L. Paulatto, C. Sbraccia, S. Scandolo, G. Sclauzero, A. P. Seitsonen, A. Smogunov, P. Umari and R. M. Wentzcovitch, *J. Phys.: Condens. Matter*, 2009, **21**, 395502.
49 P. Giannozzi, O. Andreussi, T. Brumme, O. Bunau, M. B. Nardelli, M. Calandra, R. Car, C. Cavazzoni, D. Ceresoli, M. Cococcioni, N. Colonna, I. Carnimeo, A. Dal Corso, S. de Gironcoli, P. Delugas, R. A. DiStasio, A. Ferretti, A. Floris, G. Fratesi, G. Fugallo, R. Gebauer, U. Gerstmann, F. Giustino, T. Gorni, J. Jia, M. Kawamura, H. Y. Ko, A. Kokalj, E. Kucukbenli, M. Lazzeri, M. Marsili, N. Marzari, F. Mauri, N. L. Nguyen, H. V. Nguyen, A. Otero-de-la-Roza, L. Paulatto, S. Ponce, D. Rocca, R. Sabatini, B. Santra, M. Schlipf, A. P. Seitsonen, A. Smogunov, I. Timrov, T. Thonhauser, P. Umari, N. Vast, X. Wu and S. Baroni, *J. Phys.: Condens. Matter*, 2017, **29**, 465901.
50 K. F. Garrity, J. W. Bennett, K. M. Rabe and D. Vanderbilt, *Comput. Mater. Sci.*, 2014, **81**, 446–452.
51 D. Vanderbilt, *Phys. Rev. B: Condens. Matter Mater. Phys.*, 1990, **41**, 7892–7895.

52 J. W. Bennett, D. Jones, X. Huang, R. J. Hamers and S. E. Mason, *Environ. Sci. Technol.*, 2018, **52**, 5792–5802.
53 J. W. Bennett, D. T. Jones, B. G. Hudson, J. Melendez-Rivera, R. J. Hamers and S. E. Mason, *Environ. Sci.: Nano*, 2020, **7**, 1642–1651.
54 H. J. Monkhorst and J. D. Pack, *Phys. Rev. B*, 1976, **13**, 5188–5192.
55 K. W. Corum, X. Huang, J. W. Bennett and S. E. Mason, *Mol. Simul.*, 2017, **43**, 406–419.
56 J. P. Perdew, K. Burke and M. Ernzerhof, *Phys. Rev. Lett.*, 1996, **77**, 3865–3868.
57 Z. G. Wu and R. E. Cohen, *Phys. Rev. B: Condens. Matter Mater. Phys.*, 2006, **73**, 235116.
58 A. Kokalj, *J. Mol. Graphics Modell.*, 1999, **17**, 176–179.
59 J. Towns, T. Cockerill, M. Dahan, I. Foster, K. Gaither, A. Grimshaw, V. Hazlewood, S. Lathrop, D. Lifka, G. D. Peterson, R. Roskies, J. R. Scott and N. Wilkins-Diehr, *Comput. Sci. Eng.*, 2014, **16**, 62–74.